Some Recent Investigations into Dynamics and Frictional Behavior of Pneumatic Tires

EDC Library Ref. No. 1093

DISCLAIMER

SOME RECENT INVESTIGATIONS INTO DYNAMICS AND FRICTIONAL BEHAVIOR OF PNEUMATIC TIRES

H. B. PACEJKA

Delft University of Technology, The Netherlands

ABSTRACT

A concise review of dynamic tire response to both in-plane and out-of-plane wheel motions is followed by discussions on special subjects. First, the possible self-excited in-plane motion of a wheel of which the axle is suspended with respect to the steady-moving car body is discussed. The influence of several parameters such as the rate of change of effective rolling radius with tire deflection, suspension angle, and tire torsional and slip stiffness is indicated. Second, the influence of tire inertia upon out-of-plane tire performance is elucidated on the basis of theoretical results. The experimentally observed considerable reduction of the first natural frequency of the out-of-plane motion of the tire about a diameter, due to wheel rotational speed, is analyzed. The last portion deals with a theoretical explanation of the creation of a loop in the quasi steady-state cornering force characteristic which appeared to occur on wet slippery roads with tires exhibiting certain wear patterns.

INTRODUCTION

Tire behavior may be subdivided into in-plane (symmetrical) and out-of-plane (anti-symmetrical) performance. Due to the symmetrical structure of the tire-wheel system, interaction between in-plane and out-of-plane motions may be neglected when these motions remain small. Separate treatment of both modes of motion becomes possible in that case.

At large deflections, interaction will occur. For instance, large amplitudes of the vertical motion of the wheel axle will considerably influence the average cornering stiffness of the tire (1). At large slip angles, the tire radial spring rate and deflection change. In this article these interaction effects will not be considered.

References p. 277

SOME RECENT INVESTIGATIONS INTO DYNAMICS AND FRICTIONAL BEHAVIOR OF PNEUMATIC TIRES

H. B. PACEJKA

Delft University of Technology, The Netherlands

ABSTRACT

A concise review of dynamic tire response to both in-plane and out-of-plane wheel motions is followed by discussions on special subjects. First, the possible self-excited in-plane motion of a wheel of which the axle is suspended with respect to the steady-moving car body is discussed. The influence of several parameters such as the rate of change of effective rolling radius with tire deflection, suspension angle, and tire torsional and slip stiffness is indicated. Second, the influence of tire inertia upon out-of-plane tire performance is elucidated on the basis of theoretical results. The experimentally observed considerable reduction of the first natural frequency of the out-of-plane motion of the tire about a diameter, due to wheel rotational speed, is analyzed. The last portion deals with a theoretical explanation of the creation of a loop in the quasi steady-state cornering force characteristic which appeared to occur on wet slippery roads with tires exhibiting certain wear patterns.

INTRODUCTION

Tire behavior may be subdivided into in-plane (symmetrical) and out-of-plane (anti-symmetrical) performance. Due to the symmetrical structure of the tire-wheel system, interaction between in-plane and out-of-plane motions may be neglected when these motions remain small. Separate treatment of both modes of motion becomes possible in that case.

At large deflections, interaction will occur. For instance, large amplitudes of the vertical motion of the wheel axle will considerably influence the average cornering stiffness of the tire (1). At large slip angles, the tire radial spring rate and deflection change. In this article these interaction effects will not be considered.

References p. 277

In-plane dynamic behavior of the tire-wheel system has recently become more important due to increased interest into dynamic properties of suspension-steer systems. It plays an important role in the forced excitation of steering vibrations caused by tire non-uniformity, wheel imbalance, and road unevenness.

Tire out-of-plane dynamics is of crucial importance in the same problem of steering vibrations or wheel-shimmy. Anti-symmetric tire properties determine the degree of self-excitation or negative damping about the kingpin.

In the discussion of problems which are related to the above mentioned areas, dynamic tire properties will be assumed to be linear. Material damping will be neglected. The last problem to be discussed is not of a dynamic nature, but is associated with the slow cyclic slip angle variation. Especially large slip angle amplitudes are of interest, as the frictional behavior is found to be responsible for the unusual variation of shear force vs. slip angle. This problem is essentially non-linear.

IN-PLANE DYNAMIC TIRE RESPONSE TO VERTICAL AND LONGITUDINAL AXLE MOTIONS

The discussion will be restricted to a uniform tire, rolling over a perfectly flat road. Small motions are considered in order to limit the analysis to linear response. We refer to (1) for a more complete treatment of the subject matter.

The tire model to be considered is depicted in Fig. 1. The model embodies the capability of the tire to distort in the radial and the tangential directions. The elastic tread elements enable the tire model to exhibit a deformation slip in the longitudinal direction. When the tire is distorted tangentially with respect to the wheel-rim due to a longitudinal force F_x, a large part of the tire is not deformed or is at least much less deformed than the lower portion of the tire near the contact zone. This is true when the frequency of excitation is much less than the lowest frequency of the tread band in-plane vibration.

The angular vibration of the wheel plus the effective (upper) portion of the tire mass, with respect to the footprint portion of the tread band, shows a relatively low natural frequency and plays an important role in our analysis.

Another tire property which is essential in the interaction between longitudinal and vertical motions is the variation of the effective rolling radius as a function of vertical tire deflection. A well known theory states that the effective rolling radius differs from the free outer radius because of the tangential compression of the tread band due to radial tire deflection.

When the rolling resistance is neglected, the following equations govern the in-plane response of longitudinal (F_x) and vertical (F_z) force to longitudinal (x) and vertical (z) axle displacements.

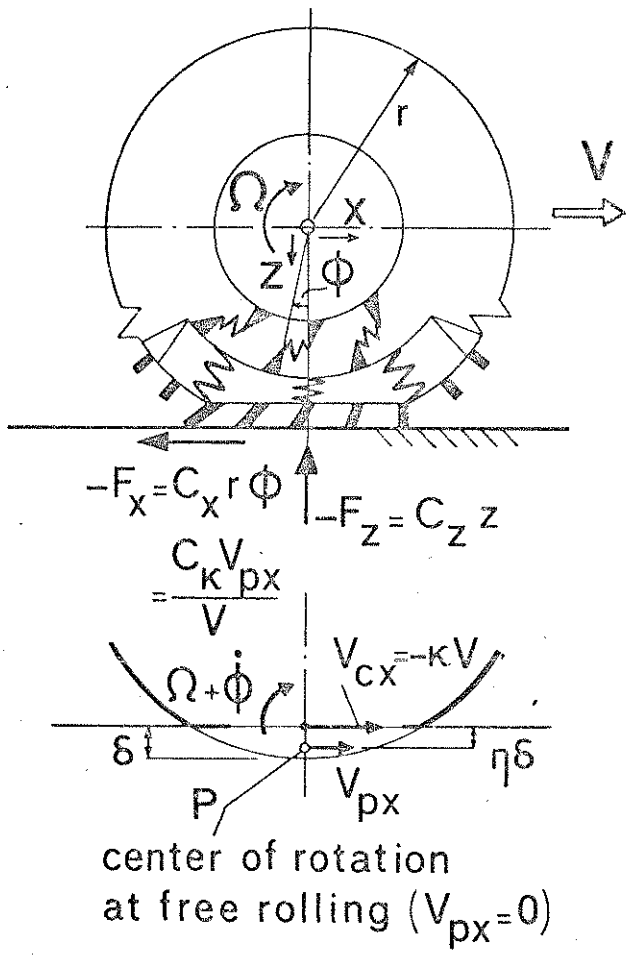

Fig. 1. In-plane tire model showing capability of carcass distortion and longitudinal slip.

The forces may be divided into a constant (average) and a variable part:

$$F_x = F_{xo} + \bar{F}_x, \quad F_z = F_{zo} + \bar{F}_z \tag{1}$$

where

$$F_{xo} = 0, \quad F_{zo} = -W_o$$

where W is the load and the index o denotes the original situation or reference value.

References p. 277

The longitudinal force is a result of the longitudinal slip of a point P, located a distance $\eta\delta$ below road level (Fig. 1) which is the center of rotation at free rolling.

$$F_x = C_\kappa\,(-V_{px}/V) = C_\kappa\left\{\kappa + (\Omega + \dot{\phi})\,\eta\,\delta/V\right\} \tag{2}$$

where C_κ denotes the longitudinal slip stiffness, V_{px} the speed of point P, V the speed of travel, Ω the rotational wheel speed, ϕ the torsion angle of the lower tread band portion with respect to the wheel-body, and δ the vertical tire deflection. The longitudinal creep or slip at road level is defined as:

$$\kappa = -\,V_{cx}/V \tag{3}$$

where V_{cx} denotes the longitudinal slip speed at road level (Fig. 1) at point C, the contact center. We have:

$$V_{cx} = V + \dot{x} - (r - \delta)\,(\Omega + \dot{\phi}). \tag{4}$$

At a particular instant, points P and C may be considered to be attached to an imaginary body which is deflected over an angle ϕ with respect to the wheel-body. Under steady state conditions, these points may be thought to be fixed to the wheel body. It may be noted that at free rolling ($F_x = 0$) and

$$\kappa = \kappa_o = -\,\eta\,\delta_o/r_{eo} \tag{5}$$

with an effective rolling radius

$$r_{eo} = V/\Omega_o = r - (1-\eta)\,\delta_o\,. \tag{6}$$

Analogous to (1) we define:

$$\kappa = \kappa_o + \bar{\kappa},\quad \Omega = \Omega_o + \bar{\Omega},\quad \delta = \delta_o + \bar{\delta}\,.$$

From (6) it follows that the effective rolling radius changes with tire deflection at a rate determined by the factor $(1 - \eta)$. If η is close to unity, the effective radius will hardly change with deflection. This is the case with radial steel belted tires. Bias-ply tires may have η values of the order of 0.5. When δ is neglected with respect to r and the relations are kept linear in the variable quantities, we obtain the following expression for F_x:

$$\begin{aligned} F_x &= C_\kappa\left\{\bar{\kappa} + \eta\bar{\delta}/r + \delta\,(\bar{\Omega} + \dot{\phi})\delta_o/V\right\} \\ &= C_\kappa\left\{(-\dot{x} + r\bar{\Omega} + r\dot{\phi})\,/\,V - (1-\eta)\,\bar{\delta}/r\right\}. \end{aligned} \tag{7}$$

The force may also be expressed in terms of the torsion angle ϕ. With C_x denoting the longitudinal stiffness of the standing tire (not including the stiffness of tread elements), we obtain:

$$F_x = -\,C_x r\phi\,. \tag{8}$$

The relation of F_x to the rotational acceleration of the wheel and effective tire mass (total polar moment of inertia: I_y) reads:

$$rF_x = -I_y\dot{\Omega}\,. \tag{9}$$

With the aid of the foregoing equations, we obtain the following differential equation for F_x as a response to the axle motions, x and z ($=\bar{\delta}$):

$$\frac{1}{C_x}\ddot{F}_x + \frac{V}{C_\kappa}\dot{F}_x + \frac{r^2}{I_y}F_x = -\ddot{x} - (1-\eta)\frac{V}{r}\dot{z}\,. \tag{10}$$

The amplitude ratios of output F_x and inputs x and z as a function of excitation frequency ω when the natural frequency $\omega_{\phi o}$ is taken to be $\omega_{\phi o} = \sqrt{(C_x r^2/I_y)}$ become:

$$\left|F_{x,x}(\omega)\right| = \frac{C_x\omega^2}{\sqrt{(\omega^2\phi_o - \omega^2)^2 + (VC_x/C_\kappa)^2\,\omega^2}} \tag{11}$$

$$\left|F_{x,z}(\omega)\right| = \frac{C_{cx}\,(1-\eta)\,(V/r)\omega}{\sqrt{(\omega^2\phi_o - \omega^2)^2 + (VC_x/C_\kappa)^2\,\omega^2}}\,. \tag{12}$$

Fig. 2 shows the above relations in graphical form for the following parameter values:

$$\begin{gathered} I_y = 0.6\ \text{kgm}^2,\ C_x = 5 \times 10^5\ \text{N/m},\ r = 0.32\ \text{m}, \\ \eta = 2/3,\ C_\kappa = 4000\ \text{N},\ \omega_{\phi o} = 92\pi\ \text{rad/s}. \end{gathered} \tag{13}$$

At low values of the frequency of excitation, ω, the response of the amplitude of F_x to x varies approximately quadratically with ω and, therefore, will become important in the higher frequency range. This is in contrast to the response to z which varies approximately linearly with ω near the origin as follows:

$$\left|F_{x,z}\,(\omega)\right|_{\omega\to o} = (1-\eta)\,I_y\,V\omega/r^3 \tag{14}$$

indicating the importance of speed, rotating mass and the factor $(1-\eta)$. The maximum of $|F_{x,z}|$ is achieved at the natural frequency $\omega_{\phi o}$. The maximum value turns out to be independent of speed V. Here, the influence of the longitudinal slip stiffness C_κ is greatest (Fig. 2).

Experiments with full scale tires confirm the trend predicted in Fig. 2 of the tire response to vertical axle motions.

The response of the vertical force, F_z, to the axle motions x and z is treated in a relatively simple manner by neglecting possible dynamic influences. The transfer functions then will read:

$$F_{z,x} = 0,\ F_{z,z} = -C_z\,. \tag{15}$$

References p. 277

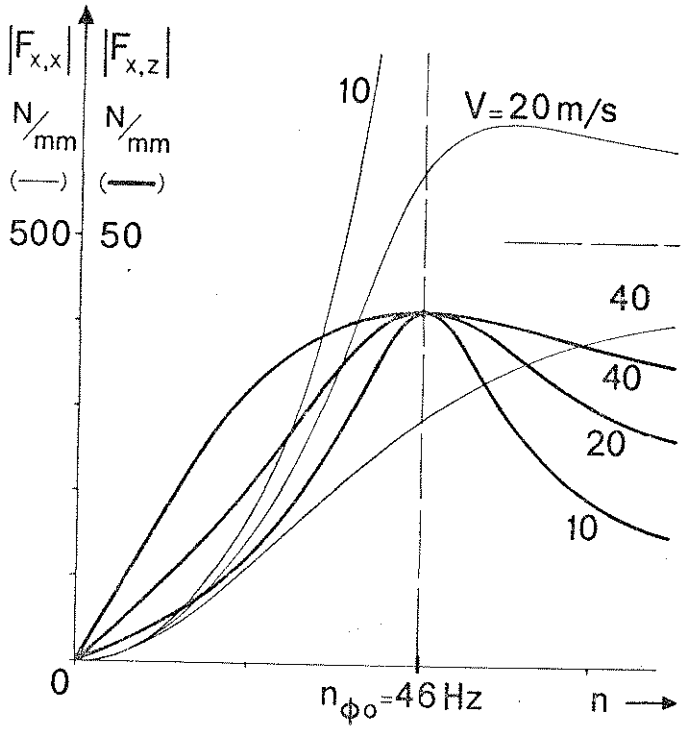

Fig. 2. Amplitude response of longitudinal force, F_x, to longitudinal axle motions, x, (thin curves) and to vertical axle motions, z, (thick curves). The parameter is the speed of travel, V.

SELF-EXCITED WHEEL BOUNCE

The wheel-suspension system to be considered is depicted in Fig. 3. The suspension angle a gives rise to a constraint relation between vertical and longitudinal axle motions:

$$x = z \tan a . \tag{16}$$

This constraint is necessary for the unstable motion to arise. The subsequent analysis makes use of the tire model discussed in the previous section.

The self-excited oscillation has been demonstrated in Professor S.K. Clark's laboratory at the University of Michigan. The phenomenon occurred with a small model tire of bias-ply construction rolling over a rotating drum. The pivot of the trailing arm was located at road level and the self-excitation showed up only at one range of speed.

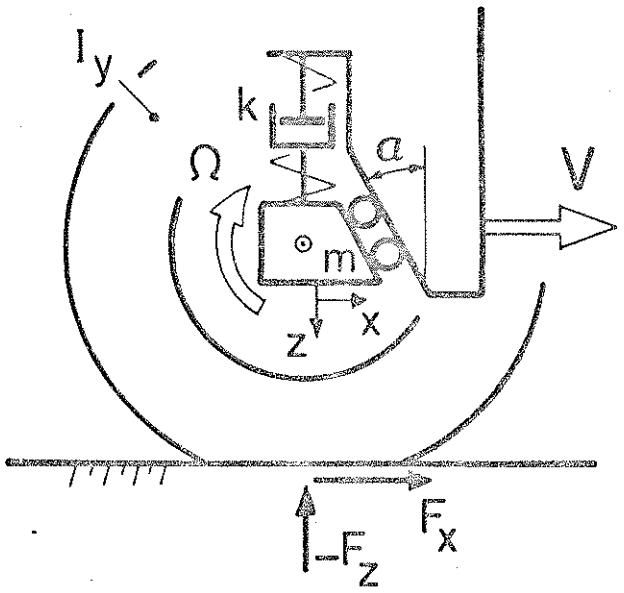

Fig. 3. Wheel-suspension system showing inclined wheel-axle guidance (angle a).

The vertical motion of the translating mass, m, is governed by the following equation

$$m^{*}\ddot{z} + k\dot{z} = F_x \tan a + F_z \tag{17}$$

with effective mass

$$m^{*} = m/\cos^2 a. \tag{18}$$

For relatively small a, this effective mass may be considered as constant.

In combination with Eqs. (10), (15) and (16), the motion is fully described. We will introduce a number of dimensionless quantities:

$$\sigma = \frac{C_x}{C_z}, \quad \tau = \frac{\omega_{\phi o}^2}{\omega_{zo}^2}, \quad \gamma = \frac{C_\kappa}{rC_x},$$

$$\beta = \frac{k}{2m^{*}\omega_{zo}}, \quad \bar{V} = \frac{V}{r\omega_{zo}}, \quad \bar{\omega}_o = \frac{\omega_o}{\omega_{zo}} \tag{19}$$

References p. 277

in which appear the natural frequencies of the undamped translation and rotation:

$$\omega 2_{zo} = \frac{C_z}{m^*}, \quad \omega 2_{\phi o} = \frac{C_x r^2}{I_y} \tag{20}$$

The characteristic equation reads ($\bar{p} = \bar{\sigma} + i\bar{\omega}_o$):

$$\bar{p}^4 + (\bar{V}/\gamma + 2\beta)\bar{p}^3 + (1 + \tau + 2\beta\bar{V}/\gamma + \bar{\sigma}\tan 2a)\bar{p}^2 + \left\{2\beta\tau + \bar{V}/\gamma + (1-\eta)\sigma\,\bar{V}\tan a\right\}\bar{p} + \tau = 0 \tag{21}$$

The conditions for stability, according to Routh-Hurwitz, reduce for the undamped system ($\beta = o$) to the following inequality:

$$\frac{1}{(1-\eta)\gamma} - (1-\eta)\gamma\sigma + \frac{\tau \cdot 1}{\tan a} + \sigma \tan a > 0 \tag{22}$$

In case Eqn. 22 is not satisfied, oscillatory instability will arise. Usually, $0 < \eta < 1$ and $\tau > 1$. For negative a, the system becomes unstable at sufficiently large values of $(1-\eta)\gamma$. Positive a, however, does not ensure stability. Large values of γ may

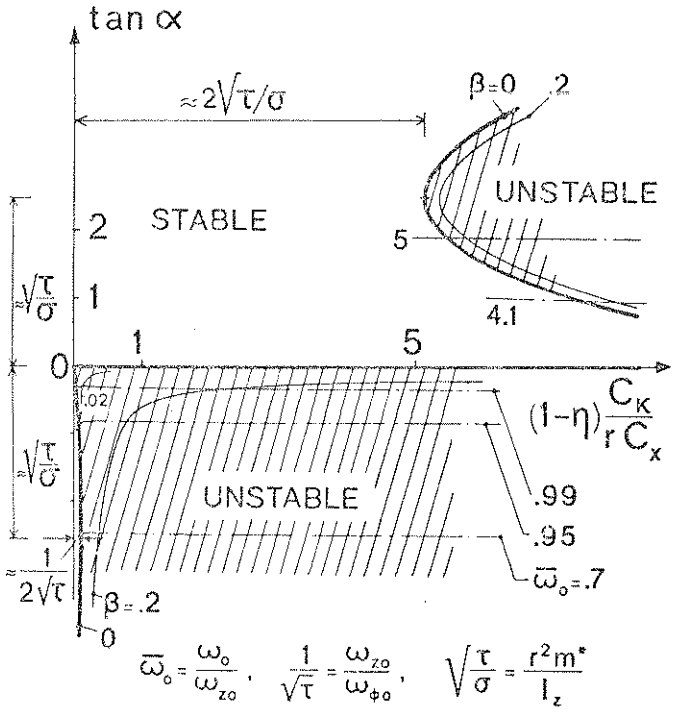

Fig. 4. Boundaries of unstable vertical wheel motions of system shown in Fig. 3.

destablize the system. A tire with η sufficiently close to unity will not be capable of showing self-excited wheel bounce.

Fig. 4 presents the stability boundaries in the parameter plane with ordinate $\tan a$ and abscissa $(1 - \eta)\gamma$. The calculations have been carried out for the following parameter values:

$$\sigma = 2.5 \quad \text{and} \quad \tau = 16 \tag{23}$$

The boundaries for the case with damping (damping ratio $\beta = 0.02$ and 0.2) hold for $\eta = 2/3$ and V = 1 (with r $\simeq$ 0.3 m and $\omega_{z0} \simeq 20\pi$ rad/s we get V = 20 m/s = 72 km/h).

The two separated unstable areas appear to represent self-excited vibrations of different modes. For positive a, the frequency of the vibration on the verge of instability (ω_0 indicated in the figure) turns out to be of the order of the natural frequency of the torsional deflection, $\omega_{\phi 0}$. For negative a, the frequency is closer to the much lower natural frequency associated with the radial deflection, ω_{z0}.

It may be noted, that a tire with the parameters specified in (13) which has a rather low value of C_κ and for which $(1 - \eta)\gamma = 1/6$, needs only little damping to avoid instability. The model aircraft tire which experienced instability had a bias-ply carcass (small η) and showed relatively stiff continuous ribs (large C_κ).

OUT-OF-PLANE DYNAMIC TIRE RESPONSE TO LATERAL AND STEER MOTIONS OF THE WHEEL AXLE

The antisymmetrical response of pneumatic tires has been a subject of study during the last three decades. Relatively recently, the mass of the tire has been included in the analysis. This extension of the well-known kinematic theories (2) is of importance, not so much to explain the phenomenon of self-excited shimmy vibrations, but to achieve a far better quantitative description of real tire behavior.

The theory of the dynamic antisymmetric response of a stretched string type tire model with mass is of considerable complexity (3). An approximate dynamic theory (4) developed recently as an extension to an earlier and simpler approximation of the dynamic influence (1), is of greater practical use. The agreement with experimental results turns out to be good (4).

The essential approximation introduced in this theory is to neglect those harmonic components of the inertial force distribution along the tire circumference that have wavelengths shorter than the circumference. This means, that the elastic deformation associated with this lateral inertial force distribution varies according to a plane. The position of this plane with respect to the wheel center plane is defined by the lateral and (two) angular displacements $(\tilde{y}_t, \tilde{\gamma}_t, \tilde{\psi}_t)$.

References p. 277

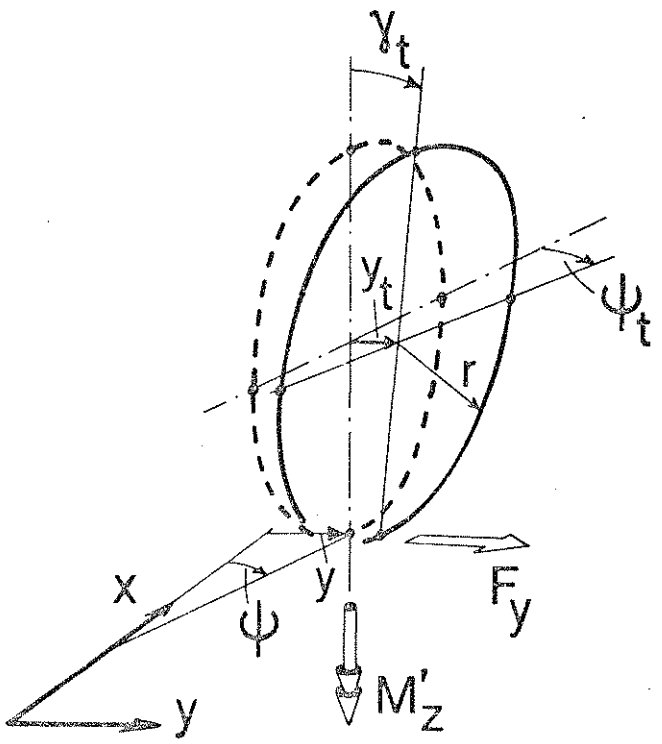

Fig. 5. Zero and first order harmonics of tire lateral distortion (= average plane distortion).

Besides these inertial forces, we have the external ground force F_y and moment M'_z (see Fig. 5) which cause the tire to distort. The zero order plus first harmonic of this "static" distortion corresponding to an inclined plane is defined by the displacements $(\overline{y}_t, \overline{\gamma}_t, \overline{\psi}_t)$. Higher harmonics do not produce a resulting force or moment acting on the wheel rim.

With C_y, C_γ, C_ψ denoting the stiffness of tire tread band with respect to wheel-rim and r the tire radius, the following relations apply:

$$\overline{y}_t = F_y/C_y, \quad \overline{\gamma}_t = -F_y r/C_\gamma, \quad \overline{\psi}_t = M'_z/C_\psi \tag{24}$$

The sum of dynamic and static deformations is denoted by (y_t, γ_t, ψ_t).

$$y_t = \overline{y}_t + \widetilde{y}_t, \quad \gamma_t = \overline{\gamma}_t + \widetilde{\gamma}_t, \quad \psi_t = \overline{\psi} + \widetilde{\psi}_t \tag{25}$$

The input motion of the wheel-plane is defined by (y, γ, ψ). Camber angle γ will be kept zero in our analysis. The input motion added to the total deformation of the

tire (y_t, γ_t, ψ_t) yields the total displacement of the tire-plane with respect to a spatial axes system. These displacements produce the inertial forces mentioned above.

With m_t, I_t and I_{tp} denoting effective tire inertia parameters and Ω the speed of revolution of the wheel, we obtain for the dynamic deformations:

$$\begin{aligned} \tilde{y}_t &= -\, m_t\,(\ddot{y} + \ddot{y}_t)\,/C_y\,, \\ \tilde{\gamma}_t &= -\left\{ I_t \ddot{\gamma}_t + I_{tp}\,\Omega\,(\dot{\psi} + \dot{\psi}_t) \right\}/C_\gamma\,, \\ \tilde{\psi}_t &= -\left\{ I_t\,(\ddot{\psi} + \ddot{\psi}_t) - I_{tp}\,\Omega\,\dot{\gamma}_t \right\}/C_\psi\ . \end{aligned} \tag{26}$$

The ground force and moment produce static deformations on top of these dynamic deformations. The generation of F_y and M_z' is considered to be the result of an effective input motion which is formed by the actual wheel-plane motion plus the dynamic deformation. By taking this effective input motion as an input to the massless kinematic theory, the approximate response of force and moment is obtained.

Instead of taking the motion of the effective wheel-plane, we may suffice with the motion of the effective line of intersection with the road plane. (cf. Fig. 6). Its location is defined by:

$$y_e = y + \tilde{y}_t - r\tilde{\gamma}_t,\ \psi_e = \psi + \tilde{\psi}_t\ . \tag{27}$$

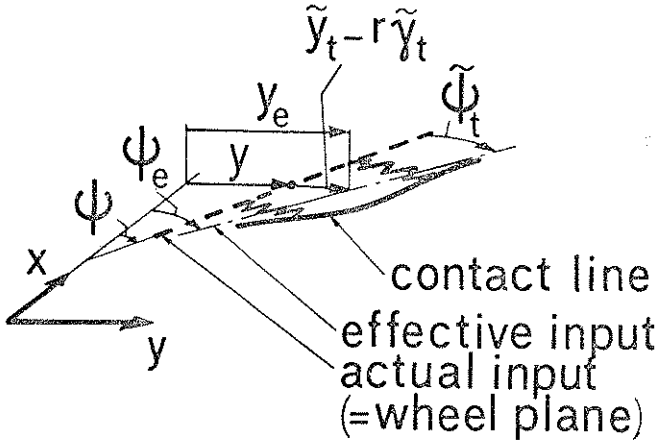

Fig. 6. Actual and effective input motion (= position of line of intersection of (effective) wheel plane and road plane).

References p. 277

We shall employ the excellent approximation of the theory of the massless string-type tire model due to von Schlippe and described in (1, 2, 3). We introduce the following quantities: 2a, the contact length between tire and road; σ, the so-called relaxation length; and C_F and C_M, the cornering and aligning stiffnesses, respectively. The frequency response functions can be written in vectorial form as a function of frequency ω:

$$(F_{y,y_e}, F_{y,\psi_e}) = \frac{C_F}{\sigma + a}\left\{(-1,0) + 1/2\,\frac{1+e^{-2i\omega\, a/V}}{1 + i\omega\sigma/V}(1,\sigma + a)\right\}$$
$$(M'_{z,y_e}, M'_{z,\psi_e}) = \frac{C_M}{a}\left\{(0,-a) + 1/2\,\frac{1-e^{-2i\omega\, a/V}}{1 + i\omega\sigma/V}(1,\sigma + a)\right\} \quad (28)$$

For practical purposes, simpler expressions may be used (3,4).

A tire which shows a finite length and width of the contact area will also generate longitudinal forces. These forces form a couple M_z^*. The sum of M'_z and M_z^* give the total moment M_z. According to a theory given in (1, 3), the frequency response function for M_z^* reads:

$$(M^*_{x,y_e}, M^*_{z,\psi_e}) = -\frac{\kappa^*}{a}\left\{1 - \frac{1 - e^{-2i\omega\, a/V}}{2i\omega\, a/V}\right\}(0,1) \quad (29)$$

with κ^* representing a tire constant.

For applications in vibratory problems associated with wheel-suspension-steer systems, it is of greater interest to know the response of force and moment acting on the assumedly rigid wheel with tire mass included. The equivalent force and moment under this condition are obtained as follows:

$$F_{y\,eq} = F_y - m_t\ddot{y}_t$$
$$M_{z\,eq} = M'_z + M^*_z - I_t\ddot{\psi}_t + I_{tp}\,\Omega\,\dot{\gamma}_t \quad (30)$$

This result should correspond to the force and moment measured in the wheel hub, $F_{y\ hub}$ and $M_{z\ hub}$, after these have been corrected for the inertial force and moment acting on the assumedly rigid wheel plus tire. With inertia parameters of wheel plus tire we find:

$$F_{y\,eq} = F_{y\,hub} + m_{wt}\ddot{y}$$
$$M_{z\,eq} = M_{z\,hub} + I_{wt}\ddot{\psi} \quad (31)$$

For the following set of parameter values measured on a radial ply steel-belted tire, a = 0.063 m, σ = 0.377 m, r = 0.322 m, C_F = 49,000 N, C_M = 1400 Nm, κ^* = 104 Nm^2, $C_\psi = C_\gamma$ = 18,100 Nm, C_y = 360,000 N/m, m_t = 5.7 kg (total mass: 8.5 kg), $I_t \simeq 1/2\ I_{tp}$ = 0.295 kgm^2. The amplitude and phase of the equivalent moment as a

response to steer angle have been computed and are shown in Fig. 7a as a function of excitation frequency $n = \omega/2\pi$. Experimentally obtained data up to a maximum of 8 Hz have been added. The phase lag occurring in the lower frequency range is responsible for the creation of self-excited wheel shimmy. The influence of tire mass is evident. Without tire mass, the same response would occur at equal wavelengths, $\lambda = V/n$, irrespective of the value of the speed of travel V.

The wavelength remains constant when the motion is excited by say a wheel imbalance ($\Omega = \omega, \lambda = 2\pi r$). The corresponding response is shown in Fig. 7b.

The resonance-frequencies, which at speeds close to zero approach a value somewhat larger than the natural frequency of the free non-rotating tire, n_{oo}, appear to separate at increasing speed. Vibration experiments performed on a free tire (not contacting the road) for the purpose of obtaining the values of certain tire parameters, gave a clear indication that a considerable reduction of the resonance-frequency may arise when the wheel spins. The next section gives a brief analysis of this phenomenon.

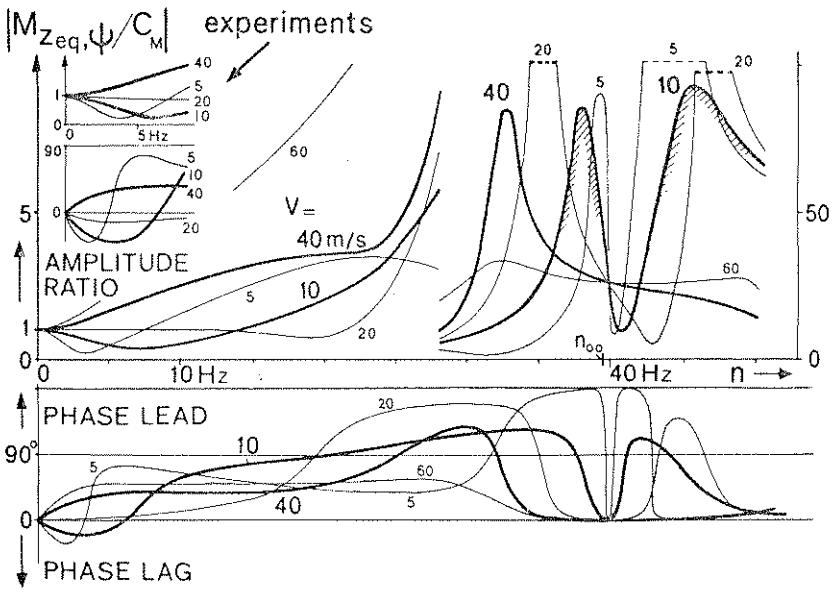

Fig. 7a. Amplitude and phase response of aligning torque to steer angle as a function of frequency of excitation. Parameter is speed of travel, V. Experimental results are given up to a frequency of 8 Hz.

References p. 277

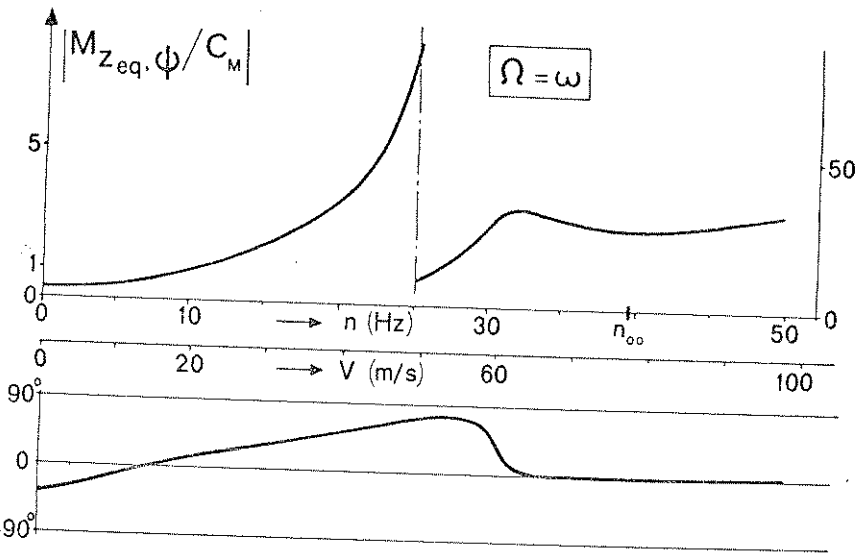

Fig. 7b. Amplitude and phase response as a function of frequency (the frequency being that of wheel revolution).

REDUCTION OF NATURAL FREQUENCY DUE TO WHEEL ROTATION

The response of a free rotating tire that is subjected to vibrations of the wheel-plane is, of course, governed by the general equations presented in the preceding section. The difference and considerable simplification in the analysis for the free rotating tire is the absence of ground force and moment. As a result of this, the static deformations vanish, and the last two equations of (26) become:

$$\begin{aligned} I_t\ddot{\gamma}_t + I_{tp}\,\Omega\,(\dot{\psi} + \dot{\psi}_t) + C_\gamma\gamma_t &= 0, \\ I_t\,(\ddot{\psi} + \ddot{\psi}_t) - I_{tp}\,\Omega\dot{\gamma}_t + C_\psi\psi_t &= 0 \quad . \end{aligned} \tag{35}$$

The free vibration of the tread band with respect to the rotating wheel-rim ($\psi = 0$) shows two natural frequencies, ω_o, which are the roots of the frequency equation:

$$\left(\frac{\omega_o}{\omega_{oo}}\right)^4 - \left\{\left(\frac{I_{tp}}{I_t}\right)^2\left(\frac{\Omega}{\omega_{oo}}\right)^2 + 2\right\}\left(\frac{\omega_o}{\omega_{oo}}\right)^2 + 1 = 0 \tag{36}$$

where

$$\omega_{oo} = \omega_{\psi oo} = \sqrt{C_\gamma/I_t} = \sqrt{C_\psi/I_t} \tag{37}$$

represents the natural frequency of the non-rotating tire ($\Omega = o$). It can be shown that with increasing Ω the natural frequencies separate more and more from the value

ω_{oo}. The lower natural frequency, which is the more important one, appears to be reduced for increasing values of Ω (Fig. 8).

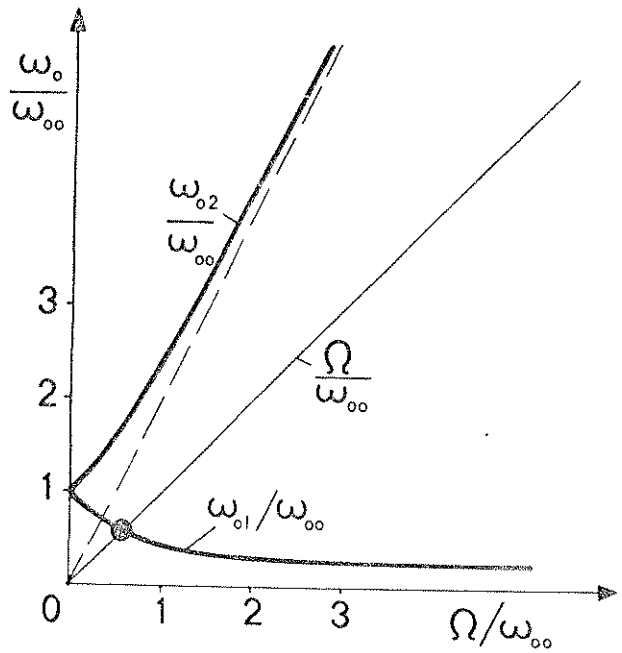

Fig. 8. Natural frequencies, ω_{o1} and ω_{o2}, as a function of rotational speed, Ω, for a free tire (not contacting the road). Camber and steer motions of the tire with respect to the rim are considered. The point where Ω reaches the value of ω_o, indicates the resonance frequency found through excitation by wheel imbalance.

When an imbalance weight excites the vibration, resonance will occur at a frequency equal to the frequency of wheel revolution, $\omega_o = \Omega$. In this particular case with the aid of this equality, the only real root of (36) becomes:

$$\omega_o = \omega_{oo} \sqrt{\frac{1 - I_{tp}/I_t}{1 - (I_{tp}/I_t)^2}}. \tag{38}$$

For the case where the effective polar moment of inertia $I_{tp} = 2\,I_t$, expression (38) reduces to

$$\omega_o \simeq 0.6\,\omega_{oo}. \tag{39}$$

References p. 277

This considerable reduction of around 40% is in excellent agreement with experimental findings. For a radial steel-belted tire, a reduction from about 40 Hz to about 25 Hz has been found.

From the equations of motion (35), it can be deduced that at $\Omega = \omega_o$, the deformation angle, γ_t, lags 90 degrees behind the angle ψ_t and 180 degrees behind the excitation angle, ψ. This agrees with experimental evidence. At $I_{tp} = 2\ I_t$, the amplitudes of γ_t and ψ_t are equal to each other. The 90 degree phase lag of γ_t with respect to ψ_t implies that an alternating deformation of the tire takes place.

SIMILARITY RULES FOR TESTING SMALL SCALE MODEL TIRES

The equations governing the dynamic performance of tires that have been derived above, may be written in dimensionless form. As a result of this, certain dimensionless numbers are recognized. These should be kept constant in order to ensure similarity between real and experimental situations.

For a small scale tire model for which geometrical similarity is to be preserved (including that of the contact zone), the ratios between various lengths must remain unchanged. If we are dealing with stiffness parameters of the mathematical tire model in the case where they almost exclusively depend on the inflation pressure, p_i, the ratio between these parameters will hardly be effected by the geometrical scaling. If p_i is not mainly responsible for the stiffness, the ratio of material elastic moduli and inflation pressure should be kept constant.

In addition, we have the following numbers, which ensure kinematic and dynamic similarity, respectively:

Kinematic Conditon:

$$\frac{\omega r}{V} = \text{constant} \tag{33}$$

Dynamic Condition:

$$\frac{\omega^2 r^2 \rho}{p_i} = \text{constant} \tag{34}$$

where ρ denotes the mass density of the tire. The kinematic condition simply states that the wavelength of the path on the road must be scaled down at the same rate as each other length parameter. The dynamic condition implies that the excitation frequency must be regarded in terms of a natural frequency of tire and model. At fixed ρ/p_i, a reduction of radius r would require an increase in excitation frequency ω while the speed V should remain unchanged. If p_i can be reduced without seriously violating the stiffness similarity condition, V and ω may be kept in an acceptable operating range.

QUASI-STATIC CYCLIC BEHAVIOR ON SLIPPERY ROADS

As has been reported earlier (5), a tire may show a non-unique cornering force vs. slip angle characteristic. An original plot is shown in Fig. 9. This phenomenon has been shown to occur on very smooth wet surfaces. The tires tested exhibited tread elements (ribs) with worn edges. This type of wear promotes the formation of a water film underneath the elements.

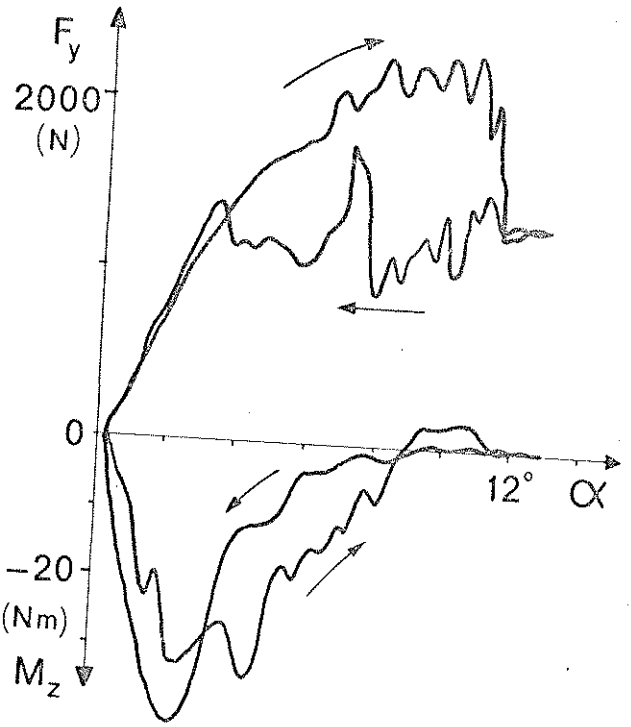

Fig. 9. Loop in quasi steady-state cornering force-slip angle relationship. Test data: Road: wet, smooth asphalt. Tire: bias-ply 5.60-13, load 400 kgf, inflation pressure 1.7 kgf/cm^2, worn edges of tread pattern ribs. Speed: 40 km/h.

The explanation of the phenomenon is not self-evident. It is rather obvious that, as a start, our model of the friction curve should drop with increasing sliding speed beyond a low speed maximum. Extensive computation reveals that this is not a sufficient conditon to get at the lower branch of the cornering force characteristic.

A second condition has been found to be necessary. The fact that the tires, which were capable of showing the loop, exhibited worn edges brought up the idea that

References p. 277

possibly a coefficient of friction, μ, arises which depends upon the orientation of the tread element relative to the road surface.

The orientation is directly related to the lateral deformation of the tire and, consequently, to the cornering force F_y. For the sake of simplicity, we have chosen a function (of speed) for the coefficient of friction which abruptly changes to an alternative representation when a critical value of the cornering force $F_{y\,crit}$ is passed (see Fig. 10).

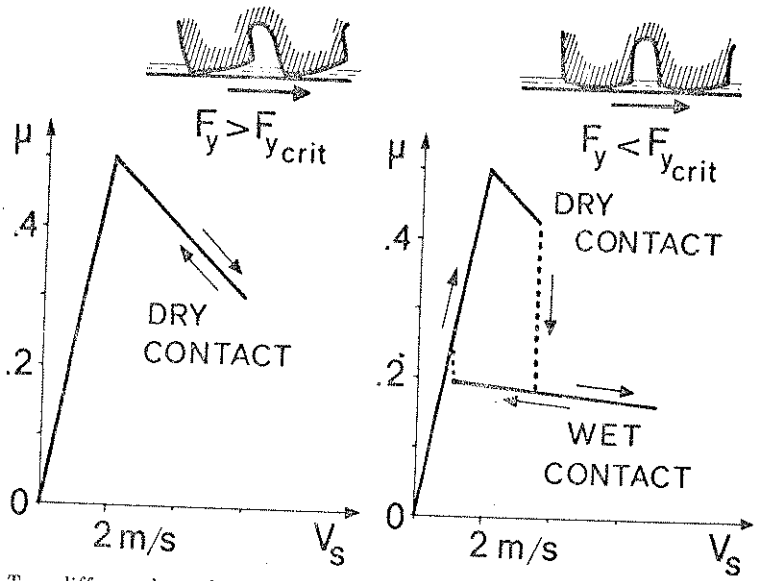

Fig. 10. Two different hypothetical wet friction functions (friction coefficient vs sliding speed). Validity depends on orientation of tread element with respect to road surface.

Mathematically, we take the following simplified friction functions (of sliding speed V_s) for the two ranges of the side force.

$$\mu = A_s V_s \quad \text{if } V_s < V_{so}$$
$$\mu = \mu_o - B_s V_s \quad \text{if } V_s > V_{so} \tag{40}$$

with parameters different for each of the distinct force ranges.

The friction properties as postulated will be applied in connection with a one-dimensional model of tire lateral elasticity represented by a Green's or influence function G (ξ,x). A lateral concentrated load acts at coordinate x and results in a lateral deformation measured at coordinate ξ (see Fig. 11).

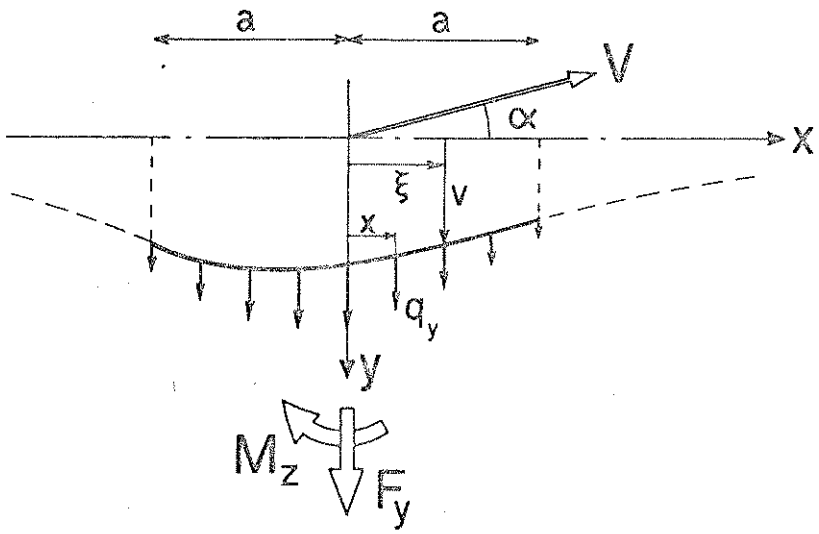

Fig. 11. Tire shear force model.

The lateral deformation, v, which is the result of a lateral force per unit length, q_y, continuously distributed over the contact length (2a), is found by means of the integral:

$$v(\xi) = \int_{-a}^{a} G(\xi,x)\, q_y(x)\, dx. \tag{41}$$

The Green's function may be obtained using the method of Savkoor (6). We shall assume a Green's function which is a symmetrical function of $x - \xi$ and which is approximated by the first two terms of the polynomial expansion of this symmetrical function:

$$G(\xi,x) = h + g(x - \xi)^2. \tag{42}$$

This approximation entails that the shape of the lateral distortion of the contact line, $v(\xi)$, becomes parabolic as well, irrespective of friction functions and vertical pressure distribution:

$$v = a_o + a_1\xi + a_2\xi^2. \tag{43}$$

To simplify the calculations, a uniform pressure distribution, $q_z = q_o$, is chosen. The lateral shear force per unit length reads:

$$q_y = \mu q_o. \tag{44}$$

References p. 277

In the contact zone, two ranges may be distinguished. In the front portion, the speed of sliding is small and does not exceed the value V_{so}. In the trailing range, the sliding speeds exceed this critical value. The point of contact where transition from one range into the other takes place, is located at coordinate x_o.

The sliding speed V_s depends on both the slip angle α, and the gradient of the lateral distortion, v:

$$V_s = V\,(\sin\alpha + \partial v/\partial\xi) \tag{45}$$

With the use of the foregoing expressions, the integral equation (41) assumes the form (for small α):

$$a_o + a_1\xi + a_2\xi^2 =$$

$$q_o\int_{-a}^{x_o} \left\{h + g\,(x-\xi)^2\right\}\left\{\mu_o - B_s V\,(\alpha + a_1 + 2a_2 x)\right\}\,dx \tag{46}$$

$$+ q_o\int_{x_o}^{a} \left\{h + g\,(x-\xi)^2\right\} A_s V\,(\alpha + a_1 + 2a_2\,x)\,dx$$

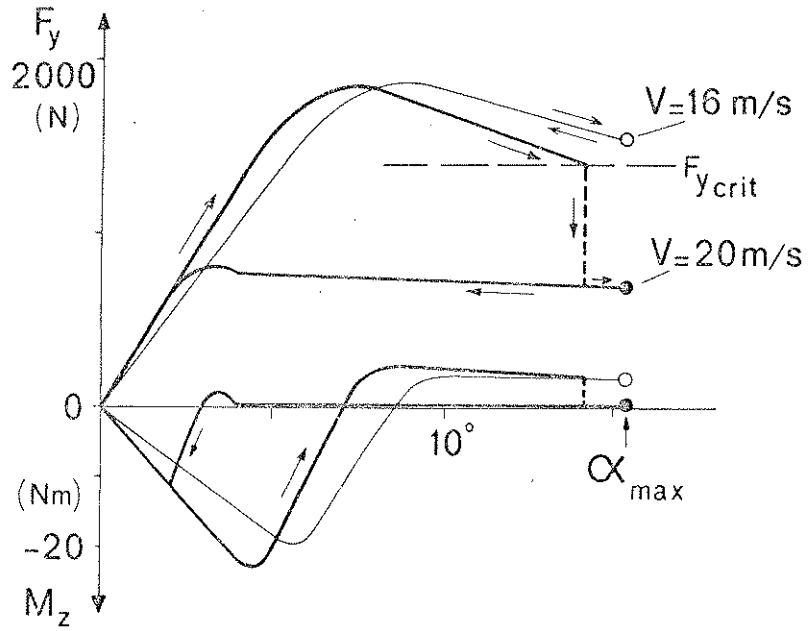

Fig. 12. Calculated side force characteristic showing jump to lower branch for a particular combination of high speed and slip angle.

Equating the coefficients of equal powers of ε in the left and right member of this equation, we obtain expressions for the unknown quantities a_0, a_1 and a_2.

Once the distortion is known, side force and aligning torque may be computed:

$$F_y = \int_{-a}^{a} q_y \, dx, \quad M_z = \int_{-a}^{a} q_y \, x \, dx \tag{47}$$

The critical value of the side force $F_{y\ crit}$ determines which portions of the friction-speed characteristics (which were calculated with both possible friction functions) are valid. A jump from the upper branch to the lower one will occur when F_y drops below $F_{y\ crit}$.

Fig. 12 shows the loop which occurs at a speed of 20 m/s with a hypothetical tire and friction model configuration with parameters:
$a = 0.1$ m, $g = -0.000125$ 1/Nm, $q_o = 20{,}000$ N/m, $F_y > F_{y\ crit}$: $\mu_o = 0.6$, $V_{so} = 2$ m/s, $A_s = 0.25$ s/m, $B_s = 0.05$ s/m, $F_y < F_{y\ crit}$: $\mu_o = 0.2$, $V_{so} = 1$ m/s, $A_s = 0.25$ s/m, $B_s = 0.005$ s/m.

At the lower speed of 16 m/s, a loop is not established for the a amplitude considered. This agrees qualitatively with experimental results (5).

REFERENCES

1. *H. B. Pacejka, "The Tire as a Vehicle Component, Yaw and Camber Analysis," Chapter 7.5 of Mechanics of Pneumatic Tires, ed. S.K. Clark, pp. 757-839, NBS Monograph 122, Washington, D.C. 1971.*
2. *B. von Schlippe and R. Dietrich, "Das Flattern eines bepneuten Rades," Bericht Lilienthal Gesellschaft 140, 1941. English translation: NACA TM 1365, p. 125, 1954.*
3. *H. B. Pacejka, "Analysis of the dynamic response of a rolling string-type tire model to lateral wheel-plane vibrations," Vehicle System Dynamics 1, pp. 37-66, 1972.*
4. *H. B. Packejka, "Approximate Dynamic Shimmy Response of Pneumatic Tires," Vehicle System Dynamics 2, pp. 49-60, 1973.*
5. *H. C. A. van Eldik Thieme, "The Tire as a Vehicle Component, Cornering and Camber Experiments," Chapter 7.3 of Mechanics of Pneumatic Tires, ed. S. K. Clark, pp. 631-693, NBS Monograph 122, Washington, D.C., 1971.*
6. *A. R. Savkoor, "The Lateral Flexibility of Pneumatic Tires and its Application to the Lateral Rolling Contact Problem," SAE Paper No. 700378, FISITA/SAE Congress, 1970.*

DISCUSSION

Clark

We have a few minutes set aside for questions.